Cell J
Cell Journal(Yakhteh)
Homepage: https://www.celljournal.org/
Original Article
Vol 26, No 2, February 2024, Pages: 130-138

Simultaneous Coating of Electrospun Nanofibers with Bioactive Molecules for Stem Cell Osteogenesis *In Vitro*

Mehrdad Zahiri-Toosi, M.Sc.[1], Seyed Jalal Zargar, Ph.D.[2]*, Ehsan Seyedjafari, Ph.D.[3], Mostafa Saberian, Ph.D.[4], Marziehsadat Ahmadi, M.Sc.[2]

1. Department of Cell and Molecular Biology, International Campus-Kish, University of Tehran, Kish Island, Iran
2. Department of Cell and Molecular Biology, School of Biology, College of Science, University of Tehran, Tehran, Iran
3. School of Biotechnology, College of Science, University of Tehran, Tehran, Iran
4. Department of Medical Laboratory Sciences, School of Allied Medical Sciences, Tehran University of Medical Sciences, Tehran, Iran

Abstract

Objective: Mesenchymal stem cells (MSCs) are widely recognized as a promising cell type for therapeutic applications due to their ability to secrete and regenerate bioactive molecules. For effective bone healing, it is crucial to select a scaffold that can support, induce, and restore biological function. Evaluating the scaffold should involve assessing MSC survival, proliferation, and differentiation. The principal aim of this investigation was to formulate composite nanofibrous scaffolds apt for applications in bone tissue engineering.

Materials and Methods: In this experimental study, nanofibrous scaffolds were fabricated using Poly-L-lactic acid (PLLA) polymer. The PLLA fibers' surface was modified by integrating collagen and hydroxyapatite (HA) nanoparticles.

Results: The findings demonstrated that the collagen- and nanohydroxyapatite-modified electrospun PLLA scaffold positively influenced the attachment, growth, and osteogenic differentiation of MSCs.

Conclusion: Coating the nanofiber scaffold with collagen and nanoparticle HA significantly enhanced the osteogenic differentiation of MSCs on electrospun PLLA scaffolds.

Keywords: Collagen, Nano-Hydroxyapatite, Tissue Engineering

Citation: Zahiri-Toosi M, Zargar SJ, Seyedjafari E, Saberian M, Ahmadi M. Simultaneous coating of electrospun nanofibers with bioactive molecules for stem cell osteogenesis in vitro. Cell J. 2024; 26(2): 130-138. doi: 10.22074/CELLJ.2024.2008921.1388

Introduction

Tissue engineering represents a highly promising approach for tissue transplantation. The initial step in engineering transplantable tissues involves the creation of scaffolds that closely mimic the biological, chemical, and mechanical properties of the extracellular matrix (ECM) (1). Three-dimensional scaffolds enable the development of *in vitro* cell cultures that resemble natural biological environments, thereby facilitating cell attachment, growth, and differentiation (2). Nanofibrous scaffolds, among the various three-dimensional scaffolds available, offer significant advantages due to their high porosity and large surface-to-volume ratio (3). Electrospinning is a commonly employed method for fabricating nanofibrous scaffolds, owing to its simplicity and cost-effectiveness (4). Furthermore, electrospun scaffolds resemble non-woven mats composed of nano-scale fibers, exhibiting structural similarities to the ECM. The ECM of bone tissue primarily consists of fibrous proteins, predominantly collagen, along with mineralized hydroxyapatite (HA) containing calcium and phosphate, which are deposited by osteocytes. A wide range of polymers is available for fabricating electrospun scaffolds with properties similar to those of the bone ECM. Additionally, there are various approaches for surface modification of the scaffolds to enhance their properties, such as surface functionalization, incorporation of natural proteins, or introduction of biochemical factors (5).

Various natural and synthetic biocompatible polymers have been extensively used for the electrospinning fabrication of nanofibrous scaffolds (6). Controlled degradation of scaffolds after transplantation into the host body is desirable. Poly-L-lactic acid (PLLA) is a widely utilized biocompatible and biodegradable polymer for scaffold fabrication in various tissue regeneration applications. However, the hydrophobic nature of PLLA limits its suitability as a cell attachment surface for nanofibrous scaffolds (7). Nevertheless, surface modification through plasma treatment has been shown to address this issue by introducing hydrophilic polar groups, thereby increasing the surface energy and facilitating better cell adhesion (8).

The application of natural bioactive macromolecules, such as collagen, to coat scaffolds stands out as a viable strategy for augmenting interactions between cells and

Received: 09/August/2023, Revised: 05/January/2024, Accepted: 21/January/2024
***Corresponding Address: P.O.Box: 141556455, Department of Cell and Molecular Biology, School of Biology, College of Science, University of Tehran, Tehran, Iran**
Email: zargar@ut.ac.ir

Royan Institute
Cell Journal (Yakhteh)

scaffolds (9). Collagen, an essential structural protein found in various tissues and notably in bone tissue as elongated fibrils, encompasses diverse isotypes. Its versatility has led to its integration into scaffold design for tissue engineering purposes. Collagen can be directly integrated into the electrospinning process, producing collagen nanofibers, or it can be chemically cross-linked with other nano-fabricated scaffolds post-electrospinning (10). The latter method yields scaffolds with enhanced mechanical properties, offering a cost-effective alternative to the use of expensive proteins. Numerous studies have illustrated that the incorporation of collagen onto electrospun fibrous scaffolds significantly amplifies the differentiation of multipotent stem cells toward osteogenic tissue (11).

HA is a mineral component that is abundantly present in bone tissue (12). HA possesses excellent osteoinductive and osteoconductive properties, making it a suitable candidate for bone regeneration and synthetic bone tissue fabrication. Various methods, such as freeze drying, 3D printing, thermally induced phase inversion, and electrospinning of HA solution in a polymer composite, have been employed for the production of porous scaffolds (13). Coating HA nanoparticles onto electrospun fibers through immersion in simulated body fluid (SBF) has also demonstrated significant advantages, potentially due to minimal interference of nano-scaled particles with the scaffold's pores and an increased surface-to-volume ratio, making these bioactive particles more accessible to cells (14).

Building upon these findings, this study aimed to prepare PLLA scaffolds through electrospinning, which were subsequently grafted with collagen type I. These grafted scaffolds were further coated with nano-HA (nHA). The osteogenic potential of the scaffolds was evaluated in comparison to pristine PLLA scaffolds and collagen cross-linked PLLA scaffolds using mesenchymal stem cells (MSCs) derived from human adipose tissue.

Materials and Methods

Scaffold preparation

This is an experimental study that as first step the scaffold was fabricated using the electrospinning technique, following a previously reported protocol (15). Briefly, a 12% (w/v) solution of PLLA (Sigma-Aldrich, MO, USA) in a mixture of dimethylformamide and chloroform (Millipore, Germany) was prepared. The solution was loaded into two 5 mL syringes and connected to a 21-gauge needle. A steel collector spinning at a rate of 400 rounds per minute was positioned 15 cm away from the needle to collect the electrospun nanofibers. The solution was sprayed using a two-syringe pump at a rate of 0.5 mL/hours with a voltage of 20 kV. The solution inside the syringes was transformed into fibers and collected by the rotating cylinder. Once the scaffold reached a thickness of approximately 200 µm, it was detached using a scalpel and placed in a hood to dry (16).

Plasma treatment of scaffold

To improve the surface hydrophilicity of the scaffolds, plasma treatment was performed. Oxygen plasma treatment was conducted using a low-frequency plasma generator (44 GHz frequency). The air was evacuated from the device, and pure oxygen was introduced into the reaction chamber at a pressure of 0.4 mbar. The glow discharge was then initiated and maintained for 10 minutes (17).

Collagen grafting

For the collagen grafting process, circular sections measuring 1.5 cm in diameter were excised from the scaffold sheets. These sections were then immersed in a solution containing N-(3-dimethylaminopropyl)-N′-ethylcarbodiimide hydrochloride (EDC) and N-hydroxy-succinimide (NHS) at a concentration of 5 mg/mL for a duration of 12 hours. Subsequently, the circular sections underwent rinsing with distilled water and were subjected to an overnight treatment with a solution of collagen type I at a concentration of 1 mg/mL. The final step involved washing the scaffolds with distilled water to eliminate any excess collagen (18).

Nano-hydroxyapatite coating

A 1% (w/v) solution of nHA was prepared by dispersing the nanoparticles in deionized water using an ultrasonic bath for 20 minutes. The plasma-treated scaffold was then immersed in the nHA aqueous suspension overnight to allow fixation of the nanoparticles on the surface of the nanofibers. Subsequently, the mat was washed with water and dried under a laminar flow. The experiments were conducted using plasma-treated PLLA, plasma-treated collagen-grafted PLLA (PLLA-CO), plasma-treated nHA-coated PLLA (PLLA-HA), and plasma-treated collagen-grafted nHA-coated PLLA (PLLA-COL-HA) (19).

Stem cell isolation and expansion

Adipose tissue was obtained from ten donors (Erma Surgical Center, Tehran, Iran) with informed consent in accordance with the guidelines of the Medical Ethics Committee (79/300942) of the Ministry of Health, Iran. The adipose tissue-derived MSCs (AD-MSCs) isolation procedure involved keeping the samples on ice in Dulbecco's Modified Eagle's Medium (DMEM) supplemented with penicillin, streptomycin, and amphotericin. The samples were treated with 0.2% collagenase II and shaken at 37°C for 30 minutes. After centrifugation at 1200 rpm for 10 minutes, the supernatant was discarded, and the cell pellet was re-suspended in DMEM supplemented with 10% (v/v) fetal bovine serum (FBS). ADSCs are cultivated in plastic flasks under standard conditions, with a temperature of 37°C and a humidified atmosphere containing 5% CO_2. Following isolation, ADSCs give rise to fibroblast-like loose colonies, consisting of spindle-shaped cells that become visible under a microscope within 1-2 days. These

colonies continue to expand, and cell proliferation leads to confluence in approximately 3-4 days. ADSCs exhibit a high proliferation rate and are subcultured once they attain 80-90% confluence. Subculturing involves washing the cells to remove the old medium and serum, followed by detachment using trypsin/EDTA. The detached ADSCs are then replated at a density of 4×10^3 cells/cm^2, requiring a period of 3 weeks for proper homogenization. It is essential to change the culture media every 3 days to maintain optimal cell growth conditions (20).

In order to induce osteogenic differentiation, the foundational medium (DMEM enriched with 10% FBS) was enhanced with 10-9 M dexamethasone, 50 µg/mL ascorbic acid 2-phosphate, and 3 mM beta-glycerophosphate (all sourced from Sigma Aldrich, USA) (21).

Mesenchymal stem cell characterization

After harvesting stem cells from adipose tissue, we evaluated their mesenchymal characteristics using two methods: flow cytometry and differentiation into the osteoblastic lineage.

Phenotyping of cell surface markers for MSCs at the second passage involved labeling with anti-human antibodies, including CD90, CD44, CD10, CD106, CD34, and CD45, using fluorescein isothiocyanate (FITC) (Beckman Coulter, Fullerton, CA). Human isotype antibodies served as controls (Becton Dickinson; Beckman Coulter).

For differentiation characterization, a density of 5×10^4 cells/ml at the second passage was cultured in a six-well plate with DMEM and 10% FBS. Upon reaching confluence within one week, the medium was replaced with osteogenic differentiation media to assess the cells' ability to differentiate into the osteoblastic lineage. This medium comprised DMEM, 50 µg/ml ascorbic acid 2-phosphate, 10 nM dexamethasone, and 10 mM β-glycerol phosphate (all obtained from Gibco, United States). Incubation occurred at 37°C with 5% CO_2 for 21 days, with medium renewal every three days. Subsequently, the cells were fixed with 10% formalin for 10 minutes, followed by staining with Alizarin Red for 20 minutes at room temperature. Finally, the cells were examined under an optical microscope, and photographic documentation was undertaken (22).

Cell treatment and osteogenic differentiation

The scaffolds were prepared as 15 mm diameter pieces and placed in 12-well tissue culture plates. To ensure sterilization, the scaffolds were immersed in 70% ethanol for 4 hours and then UV irradiation for 20 minutes (23). Cells were seeded at a density of 2×10^5 cells/cm^2 into wells harboring distinct scaffold groups, namely PLLA, PLLA-COL, PLLA-HA, and PLLA-COL-HA. Following an overnight incubation, cellular adhesion to the scaffolds was achieved, rendering them primed for treatment with a differentiation medium enriched with osteogenic factors. Throughout the differentiation period (fourteen days), the medium underwent renewal every three days (24).

Scanning electron microscopy

The scaffolds' surface morphology was scrutinized through scanning electron microscopy (SEM). To facilitate observation, the scaffolds were gold-coated using a sputter coater. Fiber diameters were determined by analyzing SEM images with image analysis software (ImageJ, NIH, USA). Furthermore, SEM was employed to investigate the morphology of AD-MSCs on the scaffolds throughout the differentiation process. Following 7 and 14 days of osteogenic differentiation, cell-loaded scaffolds underwent rinsing with phosphate-buffered saline (PBS) and fixation in a 2.5% glutaraldehyde solution for 1 hour. Subsequently, the scaffolds underwent dehydration through a series of alcohol concentration gradients and were subjected to vacuum drying (25).

Mechanical properties

The assessment of nanofibrous scaffold tensile strength was conducted utilizing a universal tensile testing machine (Galdabini, Italy). Samples measuring 10×60×0.11 mm were prepared by cutting the scaffolds, and the tensile test was executed at a crosshead speed of 50 mm/minutes under ambient conditions (26).

Cytotoxicity assessments of scaffold

The MTT assay was employed to assess the proliferation rate of MSCs on diverse scaffolds, comparing them to a non-scaffold control. MSCs were seeded onto nanofibrous scaffolds positioned in a 96-well culture plate at an initial density of 5×10^3 cells/cm^2. The cells underwent incubation at 37°C and 5% CO_2 in basal medium. At intervals of 1-, 3-, 5-, and 7-days post-seeding, 50 µL of MTT solution (5 mg/mL in PBS, from Sigma Aldrich, USA), was introduced to each well (n=3) and left to incubate at 37°C for 3.5 hours. Subsequently, the supernatant was aspirated, and 200 µL of dimethyl sulfoxide (DMSO) from Millipore, Germany, was added. Optical density measurements were recorded at 570 nm using a microplate reader (BioTek Instruments, USA) with 630 nm as the reference wavelength. The identical procedure was executed for cells cultured in the non-scaffold group, serving as the control (27).

Alkaline phosphatase activity

To assess alkaline phosphatase (ALP) activity, we extracted total protein from stem cells cultivated on both control and various scaffold substrates at three, seven, and fourteen days into the investigation. This was achieved by utilizing 200 µL of RIPA buffer. Following extraction, the lysate underwent centrifugation at 15000 rpm at 4°C for 15 minutes to segregate cellular debris. The resulting supernatant was then gathered, and the ALP activity was gauged using an ALP assay kit (Pars Azmun, Iran). The enzyme's activity (IU/L) was subsequently normalized relative to the total protein concentration (mg/dL) (28).

Calcium content assay

Calcium deposition across both the control and all samples was assessed by introducing cresol phthalein reagent into the calcium solution. To elicit calcium extraction, scaffolds underwent treatment with 0.6 N HCl (Millipore, Germany), with continuous agitation at 4°C for a duration of 4 hours. The optical density was gauged at 570 nm, and the calcium content was extrapolated from the standard curve provided by the kit (Pars Azmun, Iran), utilized as a benchmark reference (29).

Statistical analysis

Each measurement was conducted in triplicate, and the findings are expressed as mean ± standard deviation. Statistical comparison of the results employed one-way and two-way analysis of variance (ANOVA), with statistical significance set at a $P<0.05$. The statistical analyses were executed utilizing GraphPad Prism software, version 9 (GraphPad Software Company, USA).

Results

Characterization of scaffolds

The electrospun PLLA nanofibrous scaffolds were examined using SEM to evaluate their structural characteristics. Figure 1A displays the morphology of the scaffolds without collagen coating, revealing a dense network of nanoscale fibers with an average diameter of 689 ± 32 nm and a random orientation. In Figure 1B, the scaffolds were grafted with collagen, resulting in a more interconnected and three-dimensional architecture compared to the non-coated scaffolds. The collagen grafting enhanced the overall scaffold structure, promoting better cell adhesion and potential for tissue integration. Figure 1C represents the scaffolds that were simultaneously coated with collagen and HA. The SEM image demonstrates the presence of both collagen fibers and HA clusters, forming a composite structure. The incorporation of HA provides the scaffold with enhanced bioactivity and potential for supporting bone regeneration. The nanoscale fiber composition, random orientation, and the presence of collagen and HA make these scaffolds promising candidates for various biomedical applications.

The affirmation of collagen presence on PLLA fiber surfaces was validated through Attenuated Total Reflectance-Fourier Transform Infrared (ATR-FTIR) spectroscopy, as depicted in Figure 2. The ATR-FTIR spectrum distinctly displayed peaks at 1633 and 1531 cm^{-1}, indicative of amide bonds within collagen residues (Fig.2, red). These peaks align with well-documented absorption bands associated with collagen in existing literature (30). Specifically, the 1633 cm^{-1} peak corresponds to the stretching vibration of the C=O bond (amide I band), while the 1531 cm^{-1} peak corresponds to the bending vibration of the N-H bond (amide II band) in collagen. These observations strongly support the effective integration of collagen onto the PLLA fiber surface.

Tensile measurements were conducted to assess the mechanical properties of the scaffolds, providing valuable insights into their structural integrity and potential for supporting tissue regeneration. The results revealed a consistent strength of 1.84 ± 0.01 MPa, highlighting the scaffold's robustness and ability to withstand applied forces. Moreover, the scaffolds exhibited an impressive elongation at break of 84%, signifying their exceptional flexibility and capacity to accommodate mechanical stresses without compromising structural integrity.

In this study, the examination of the porous configuration of the scaffolds demonstrated no considerable hindrance subsequent to collagen grafting, regardless of the presence or absence of nHA coating (Fig.1B, C). The integrity of scaffold porosity was preserved, facilitating effective fluid exchange and potential cellular penetration. Remarkably, a uniform dispersion of nHA particles was evident upon visual inspection of the surfaces of the collagen-grafted nanofibers (Fig.1C).

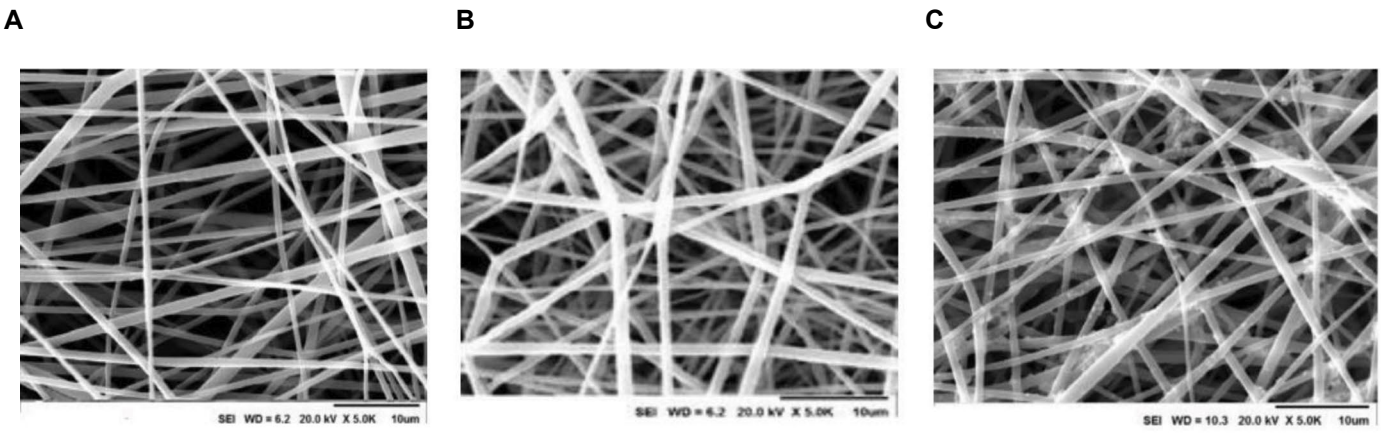

Fig.1: Scanning electron microscopy (SEM) micrographs depicting the morphology of electrospun Poly-L-lactic acid (PLLA) nanofibrous scaffolds (scale bar is 10 µm, magnification 5000x). **A.** PLLA scaffold without collagen coating, **B.** PLLA scaffold grafted with collagen, and **C.** PLLA scaffold simultaneously coated with collagen and hydroxyapatite (HA).

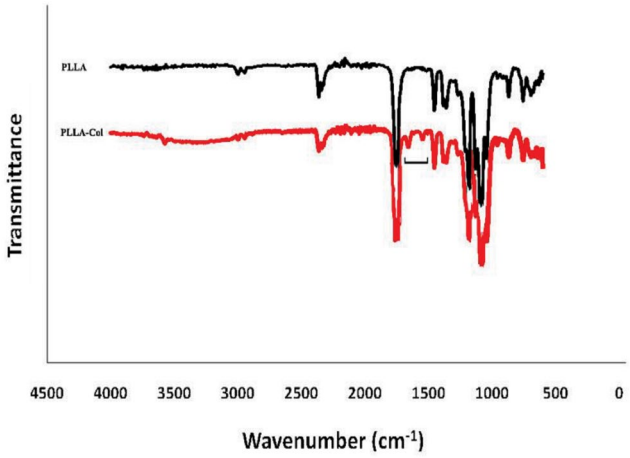

Fig.2: ATR-FTIR analysis of Poly-L-lactic acid (PLLA) (black) and collagen-coated PLLA fibers (red) revealing molecular interactions and structural changes. As shown in the chart, there are peaks at wavelengths 1633 and 1531 cm^{-1}. These peaks are related to amide groups, which are characteristic of the presence of collagen in the scaffold structure.

Biocompatibility of scaffolds

The biocompatibility of the scaffolds was evaluated using the MTT assay on day 1 of cell seeding (Fig.3A). The results showed no significant difference in viability between all the scaffolds and the control. Furthermore, the biocompatibility of the scaffolds was assessed in 3,5 and 7 days after seeding by the MTT assay (Fig.3B). The findings revealed an increased rate of MSC proliferation on third to seventh days, without any significant increase in cell number among with control in all groups scaffolds. Gradual proliferation continued on the control and all scaffolds until day five. MSCs seeded on these different groups exhibited a higher proliferation rate compared to previous days. However, the highest number of stem cells was observed on PLLA-COL-HA and PLLA-COL scaffolds at the end of day seven. All values are presented as mean ± SD. Statistical analysis was performed using two-way ANOVA, and a $P<0.05$ was considered significant.

Mesenchymal stem cell characterization

Verification of the osteogenic differentiation pathway in MSCs was executed by employing Alizarin red staining following a fourteen days culture in osteogenic-defined media (Fig.4A). Upon scrutiny of cell surface markers via flow cytometry, it was discerned that the isolated cells manifested positive expression for CD10, CD44, CD90, and CD106 markers. In contrast, the markers CD34 and CD45, signifying a hematopoietic lineage, exhibited a negative response (Fig.4B).

The morphology of MSCs, their attachment (Fig.5A, B), and the mineralization on their surfaces were visualized through SEM. While a quantitative assessment of mineralization was not achievable, the outcomes unequivocally indicated the initiation of osteogenesis (Fig.5C).

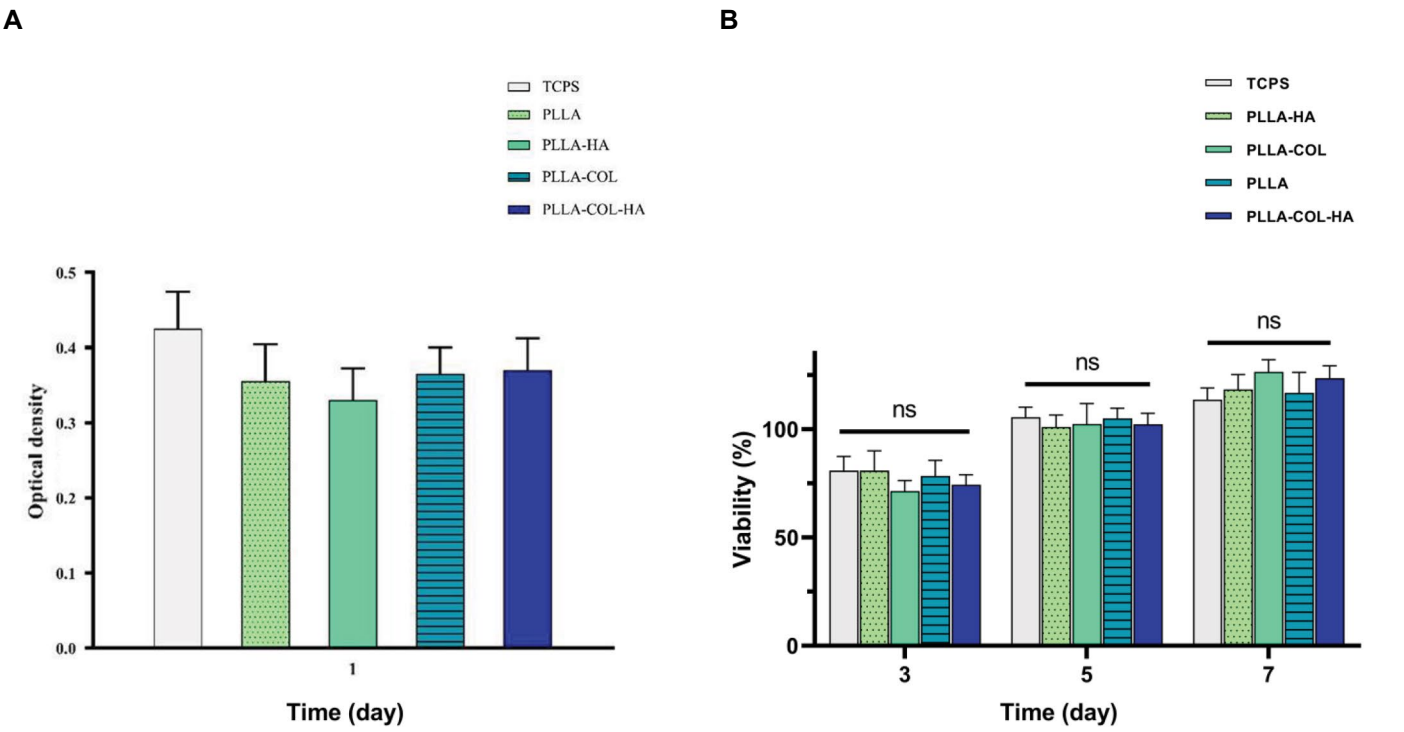

Fig.3: Comparison of cell viability rates between various scaffolds and TCPS. **A.** Comparison of cell viability rates between various scaffolds and TCPS. Evaluation of scaffold's cell-capturing capability using MTT Assay on day 1 of cell seeding. There is no significant difference in cell viability between all the scaffolds and the TCPS groups. **B.** The findings demonstrate a lack of statistically significant differences among the groups. Over the temporal progression from the third day to the fifth and seventh days, a notable augmentation in cell numbers is observed, indicative of cell proliferation across all scaffold cohorts when juxtaposed with the control. Consequently, the evident biocompatibility of the scaffolds is consistent across all experimental groups (significant criterion $P<0.05$). TCPS; Tissue culture polystyrene, PLLA; Poly-l-Lactic Acid, HA; Hydroxyapatite, COL; Collagen, and ns: Non-significance.

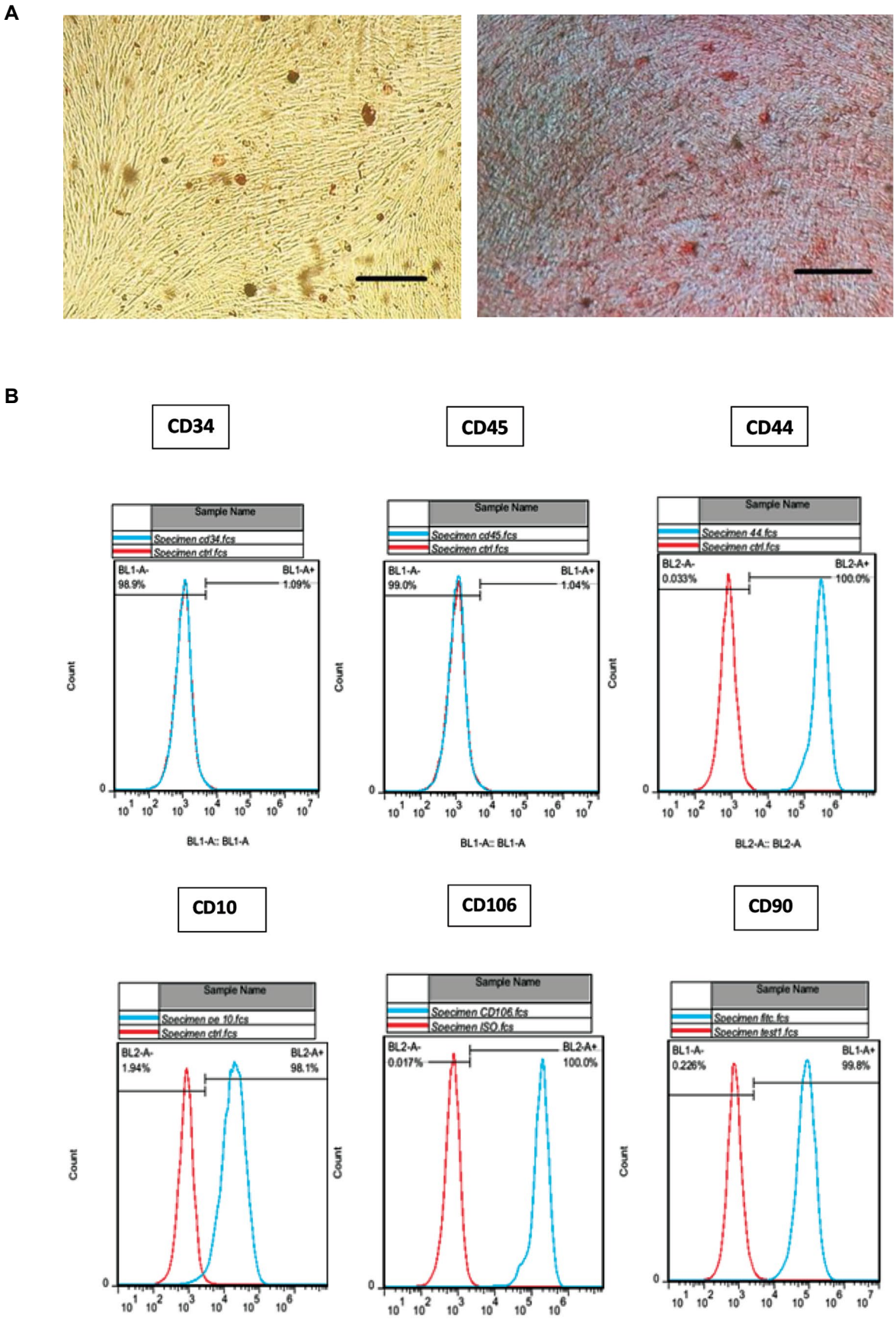

Fig.4: Mesenchymal stem cell characterization. **A.** Alizarin Red staining on day 14 reveals calcium deposits in osteogenically treated cells (10x magnification, scale bar: 50 µm) for fourteen days. Left; Basal medium, Right; Osteogenic differentiation medium underscores the successful initiation or accumulation of calcium mineralization (scale bar: 50 µm). **B.** Phenotyping of cell surface markers for MSCs at the second passage involved labeling with anti-human antibodies, including CD90, CD44, CD10, CD106, CD34, and CD45, using FITC. MSCs; Mesenchymal stem cells.

Osteogenic differentiation (alkaline phosphatase activity and calcium content)

To further explore the capacity of electrospun PLLA and other composite scaffolds in facilitating the osteogenic differentiation of MSCs, assessments were made for ALP activity (Fig.6A) and calcium content (Fig.6B). Across all scaffolds, including the control group, a consistent pattern in ALP activity was observed. On day seven, all groups exhibited the highest ALP activity, with PLLA-COL-HA, PLLA-HA, and PLLA-COL scaffolds demonstrating elevated ALP levels, and no statistically significant differences noted between these groups (P>0.05).

Mineralization or calcium content quantification occurred on days 7, 14, and 21 post cell seeding. Elevated calcium levels were evident on PLLA-COL-HA and PLLA-HA scaffolds compared to PLLA and the control on day 7. Subsequently, on days 14 and 21, the calcium content in PLLA-COL-HA, PLLA-HA, and PLLA-COL scaffolds exhibited a statistically significant increase compared to the PLLA and control groups (P<0.05, Fig.6B). The data are presented as mean ± standard deviation (SD), and statistical analysis employed one-way analysis of variance (ANOVA), with significance considered at a P<0.05.

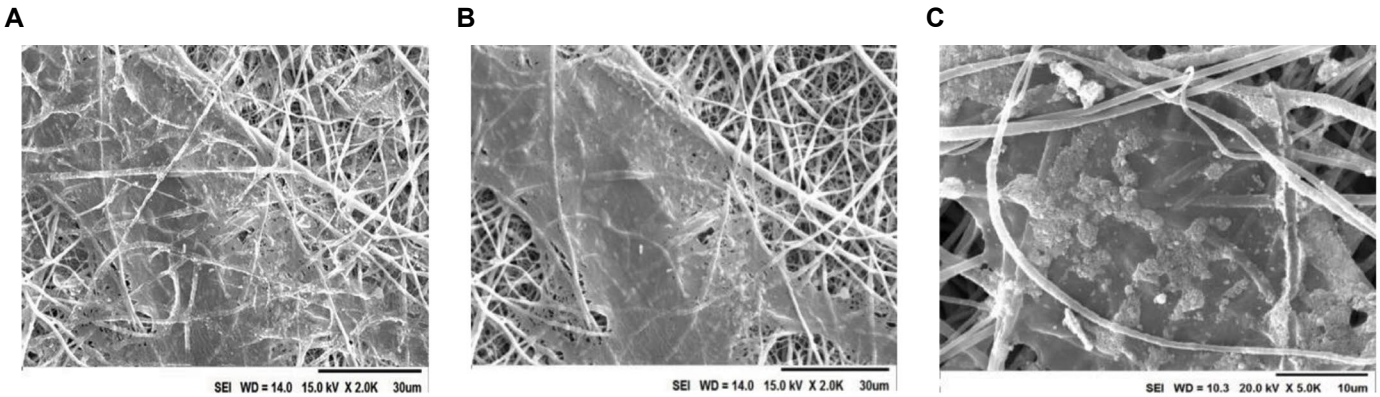

Fig.5: SEM images of MSCs expanded on scaffolds on the fourteenth day. **A.** Poly-lactic acid scaffold with hydroxyapatite nanoparticles at a magnification of 2000x, and **B.** poly-lactic acid scaffold with collagen coating at a magnification of 2000x. **C.** Poly-lactic acid scaffold with collagen coating and hydroxyapatite nanoparticles at a magnification of 5000x. To enhance visual clarity, this image has been deliberately chosen with an increased level of magnification. SEM; Scanning electron microscopy and MSCs; Mesenchymal stem cells.

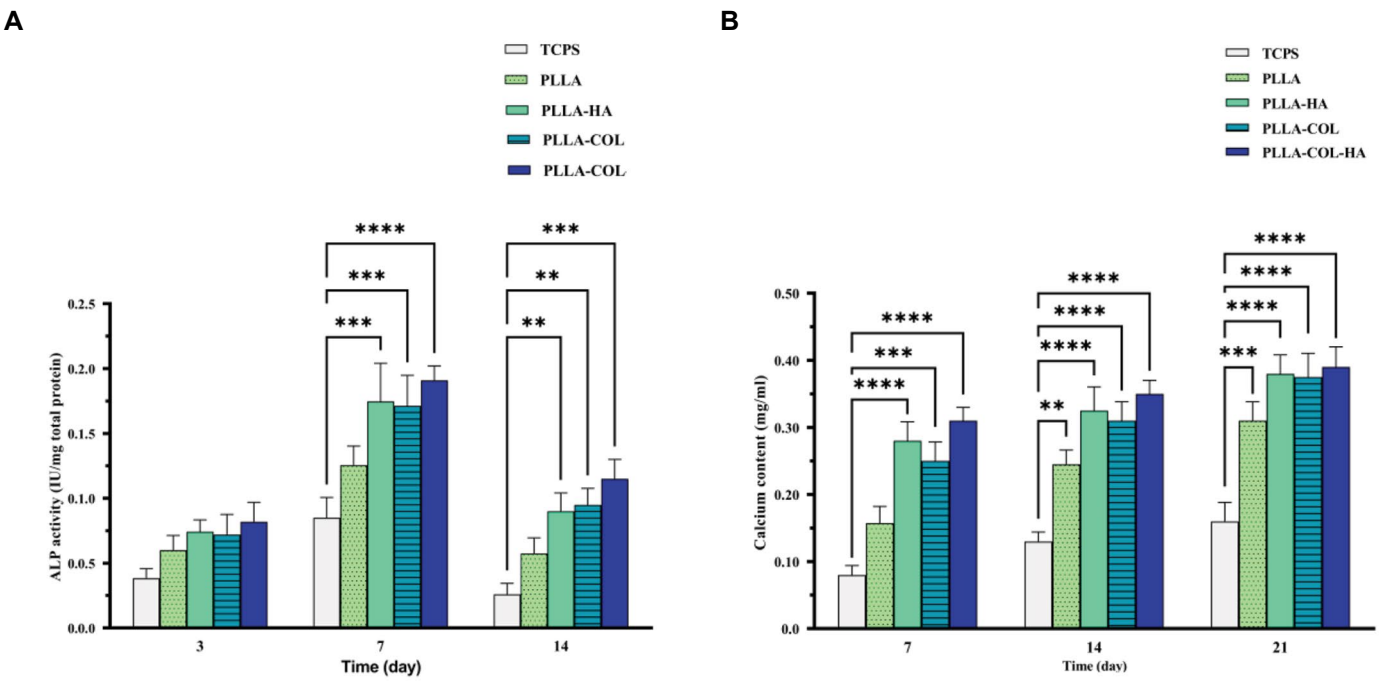

Fig.6: Osteogenic differentiation of mesenchymal stem cells. **A.** Alkaline phosphatase (ALP) activity of MSCs on days 3, 7, 14. ALP activity of mesenchymal stem cells (MSCs) on days 3, 7, and 14 to assess osteogenic differentiation on electrospun poly-L-lactic acid (PLLA) and composite scaffolds. The highest ALP activity was observed on day seven in all groups, with PLLA-COL-HA, PLLA-HA, and PLLA-COL scaffolds exhibiting comparatively higher ALP activity, with significant differences between these groups comparing control group. **B.** The quantification of mineralization or calcium content was assessed on days 7, 14, and 21 following cell seeding. On day 7, higher levels of calcium were observed in the PLLA-COL-HA and PLLA-HA scaffolds compared to PLLA and the control group. Furthermore, on days 14 and 21, the amount of calcium in the PLLA-COL-HA, PLLA-HA, and PLLA-COL scaffolds was significantly higher compared to the PLLA and control groups. **; P<0.01, ***; P<0.001, and ****; P<0.0001.

Discussion

In recent years, the burgeoning demand for bone substitutes in clinical settings has necessitated advancements in bone tissue engineering (31). A predominant focus in this domain has been the replication of the bone ECM. As an embodiment of this initiative, there has been considerable interest in integrating bioceramics with biocompatible scaffolds (32).

Despite the intrinsic properties of PLLA scaffolds resembling the ECM of bone tissue, inherent limitations challenge their application in tissue engineering. To address this, we developed PLLA scaffolds that were both grafted with collagen and coated with nHA, ensuring a uniform distribution of nHA, preventing pore blockage, and facilitating nutrient transport. Our findings are particularly significant in this context, as our developed scaffolds, when coated with bioceramics, have been efficacious in promoting osteogenic differentiation (33). This assertion finds support in the ATR-FTIR spectrum, where characteristic peaks evidencing the presence of collagen were detected, corroborating the successful surface modification of the PLLA fibers. The findings strongly support the effective integration of collagen onto the PLLA fiber surface and reveal that PLLA-COL, PLLA-nHA, and PLLA-COL-nHA scaffolds exhibited significantly enhanced stem cell proliferation compared to basic PLLA scaffolds. The results of evaluating ALP groups that include hydroxyapatite, especially in the PLLA-nHA and PLLA-CO-nHA configurations. Upon examination of cell surface markers using flow cytometry, it was observed that the isolated cells demonstrated positive expression for CD10, CD44, CD90, and CD106 markers. Conversely, markers CD34 and CD45, indicative of a hematopoietic lineage, showed a negative response (34). This underscores the potential of these advanced scaffolds in bone tissue engineering. Furthermore, Yanagida's pioneering work on HAp nanocrystal-coated PLLA demonstrated successful implant materials with reduced inflammation and improved cell adhesion, showcasing promise for soft tissue-compatible and bioabsorbable scaffolds. Similarly, Liao's (34) study on biodegraded nHAC composites highlighted increased neutrophil responses, emphasizing the need for further *in vivo* analyses to assess the regenerative efficacy of scaffolds addressing critical-size bone defects. These collective findings contribute to advancing the understanding and potential applications of innovative biomimetic materials in the field of tissue engineering. Such findings mirror prior research where collagen was effectively affixed to various scaffolding materials, subsequently amplifying their biocompatibility and fostering cell adhesion (35).

The intricate initiation of osteogenesis in the presence of nHA coating on PLLA involves complex factors including biomineralization, osteoconductive properties, signaling cues, and optimized interactions between cells and the material. We note that nHA precipitates HA crystal deposition, emulating organic mineralization (36). Furthermore, its osteoconductive faculties champion osteogenic cell adhesion and migration (37), and the ion release from nHA acts as pivotal signaling entities, catalyzing osteogenic differentiation (38). The resulting synergy between nHA and PLLA enriches cell-material interactions, thereby energizing osteogenic differentiation pathways.

The outcomes of assessing ALP levels and calcium content indicate a progressive augmentation over time in ALP enzyme and calcium production across all experimental groups. Nevertheless, a more pronounced elevation is observed in groups incorporating hydroxyapatite, particularly in PLLA-nHA and PLLA-CO-nHA configurations. This outcome substantiates earlier investigations highlighting the significant impact of HA nanoparticles on osteogenesis. Notably, within the hydroxyapatite-integrated groups, the PLLA-CO-nHA group exhibits superior ossification. Previous research has unequivocally established the favorable influence of collagen grafting on osteogenesis (39). Hence, the heightened ossification observed can be attributed to the structural intricacies, activation of cell signaling subsequent to surface adhesion, optimal mechanical resilience, and the concurrent increase in ALP and calcium deposition, aligning with established principles in the field (40).

Conclusion

The innovative combination of coating PLLA nanofibers with nHA in conjunction with collagen grafting introduces a novel approach that not only fosters the proliferation of MSCs but also promotes their osteogenic differentiation, making it a promising strategy for bone tissue engineering applications. These findings underscore the effectiveness of collagen grafting and nHA coating in augmenting both the surface properties and osteogenic potential of PLLA nanofibrous scaffolds, further establishing their utility in bone tissue engineering. The MSCs demonstrate the capability to release bioactive molecules conducive to tissue regeneration. However, comprehensive *in vivo* analyses are imperative to assess the regenerative efficacy of scaffolds incorporating nHA/PLLA, collagen/PLLA, and collagen/nHA/PLLA in addressing critical-size bone defects.

Acknowledgements

The authors gratefully acknowledge the financial support provided by the Stem Cell Technology Research Center, Tehran, Iran, for making this research possible. We would like to express our appreciation to the staff and researchers at the Stem Cell Technology Research Center for their valuable guidance and assistance throughout this study. The authors declare no conflicts of interest associated with this research study.

Authors' Contributions

S.J.Z., E.S.J., M.S.; Conceptualization, Methodology, and Software. S.J.Z.; Data curation and Supervision.

M.Z.-T.; Writing-Original draft preparation and Investigation. M.S.; Visualization. M.S.A.; Software and Validation. E.S.J.; Writing- Reviewing and Editing. All authors read and approved the final manuscript.

References

1. Rickel AP, Deng X, Engebretson D, Hong Z. Electrospun nanofiber scaffold for vascular tissue engineering. Mater Sci Eng C Mater Biol Appl. 2021; 129: 112373.
2. Zhang Q, Li M, Hu W, Wang X, Hu J. Spidroin-based biomaterials in tissue engineering: general approaches and potential stem cell therapies. Stem Cells Int. 2021; 2021: 7141550.
3. Zamani D, Moztarzadeh F, Bizari D. Alginate-bioactive glass containing Zn and Mg composite scaffolds for bone tissue engineering. Int J Biol Macromol. 2019; 137: 1256-1267.
4. Lim DJ. Bone mineralization in electrospun-based bone tissue engineering. Polymers (Basel). 2022; 14(10): 2123.
5. Doostmohammadi M, Forootanfar H, Ramakrishna S. Regenerative medicine and drug delivery: Progress via electrospun biomaterials. Mater Sci Eng C Mater Biol Appl. 2020; 109: 110521.
6. Biswal T, BadJena SK, Pradhan D. Sustainable biomaterials and their applications: a short review. Mater Today Proc. 2020; 30: 274-282.
7. Biswal T. Biopolymers for tissue engineering applications: a review. Mater Today Proc. 2021; 41: 397-402.
8. Amani H, Arzaghi H, Bayandori M, Dezfuli AS, Pazoki-Toroudi H, Shafiee A, et al. Controlling cell behavior through the design of biomaterial surfaces: a focus on surface modification techniques. Adv Mater Interfaces. 2019; 6(13): 1900572.
9. Abbasian M, Massoumi B, Mohammad-Rezaei R, Samadian H, Jaymand M. Scaffolding polymeric biomaterials: Are naturally occurring biological macromolecules more appropriate for tissue engineering? Int J Biol Macromol. 2019; 134: 673-694.
10. Tavia W, Smart multifunctional sutures for advanced healthcare. 2020. https://dspace.library.uvic.ca/handle/1828/12121 (9 Aug 2023).
11. Nammian P, Asadi-Yousefabad SL, Daneshi S, Sheikhha MH, Tabei SMB, Razban V. Comparative analysis of mouse bone marrow and adipose tissue mesenchymal stem cells for critical limb ischemia cell therapy. Stem Cell Res Ther. 2021; 12(1): 58.
12. Pang Y, Li D, Zhou J, Liu X, Li M, Zhang Y, et al. In vitro and in vivo evaluation of biomimetic hydroxyapatite/whitlockite inorganic scaffolds for bone tissue regeneration. Biomed Mater. 2022; 17(6).
13. Fu Z, Cui J, Zhao B, Shen SG, Lin K. An overview of polyester/hydroxyapatite composites for bone tissue repairing. J Orthop Translat. 2021; 28: 118-130.
14. Shaker M, Yaghmaee MS, Shahalizade T, Ghazvini AAS, Riahifar R, Raissi B, et al. Prediction of the lithium storage capacity of hollow carbon nano-spheres based on their size and morphology. J Mater Sci: Mater Electron. 2022; 33: 12760-12770.
15. Xue J, Pisignano D, Xia Y. Maneuvering the migration and differentiation of stem cells with electrospun nanofibers. Adv Sci (Weinh). 2020; 7(15): 2000735.
16. Fu Z, Li D, Lin K, Zhao B, Wang X. Enhancing the osteogenic differentiation of aligned electrospun poly(L-lactic acid) nanofiber scaffolds by incorporation of bioactive calcium silicate nanowires. Int J Biol Macromol. 2023; 226: 1079-1087.
17. Asadian M, Chan KV, Norouzi M, Grande S, Cools P, Morent R, et al. Fabrication and plasma modification of nanofibrous tissue engineering scaffolds. Nanomaterials (Basel). 2020; 10(1): 119.
18. Bazrafshan Z, Stylios GK. Spinnability of collagen as a biomimetic material: a review. Int J Biol Macromol. 2019; 129: 693-705.
19. Bordea IR, Candrea S, Alexescu GT, Bran S, Băciuț M, Băciuț G, et al. Nano-hydroxyapatite use in dentistry: a systematic review. Drug Metab Rev. 2020; 52(2): 319-332.
20. Araña M, Mazo M, Aranda P, Pelacho B, Prosper F. Adipose tissue-derived mesenchymal stem cells: isolation, expansion, and characterization. Methods Mol Biol. 2013; 1036: 47-61.
21. Bunnell BA. Adipose tissue-derived mesenchymal stem cells. Cells. 2021; 10(12): 3433.
22. Saberian M, Shahidi Delshad E. The role of Spirulina platensis on the proliferation of rat bone marrow-derived mesenchymal stem cells. Iran J Microbiol. 2023; 15(1): 111-120.
23. Niemczyk-Soczynska B, Kolbuk D, Mikulowski G, Ciechomska IA, Sajkiewicz P. Methylcellulose/agarose hydrogel loaded with short electrospun PLLA/laminin fibers as an injectable scaffold for tissue engineering/3D cell culture model for tumour therapies. RSC Adv. 2023; 13(18): 11889-11902.
24. Shafaei H, Kalarestaghi H. Adipose-derived stem cells: an appropriate selection for osteogenic differentiation. J Cell Physiol. 2020; 235(11): 8371-8386.
25. Raja IPS, Lee SH, Kang MS, Hyon SH, Selvaraj AR, Prabakar K, et al. The predominant factor influencing cellular behavior on electrospun nanofibrous scaffolds: Wettability or surface morphology? Mater Des. 2022; 216(19): 110580.
26. Nuge T, Tshai KY, Lim SS, Nordin N, Hoque ME. Characterization and optimization of the mechanical properties of electrospun gelatin nanofibrous scaffolds. World J Eng. 2020; 17(1): 12-20.
27. Saberian M, Seyedjafari E, Zargar SJ, Mahdavi FS, Sanaei-rad P. Fabrication and characterization of alginate/chitosan hydrogel combined with honey and aloe vera for wound dressing applications. J Appl Polym Sci. 2021; 138(47): 51398.
28. Jaroszewicz J, Idaszek J, Choinska E, Szlazak K, Hyc A, Osiecka-Iwan A, et al. Formation of calcium phosphate coatings within polycaprolactone scaffolds by simple, alkaline phosphatase based method. Mater Sci Eng C Mater Biol Appl. 2019; 96: 319-328.
29. Azadian E, Arjmand B, Ardeshirylajimi A, Hosseinzadeh S, Omidi M, Khojasteh A. Polyvinyl alcohol modified polyvinylidene fluoride-graphene oxide scaffold promotes osteogenic differentiation potential of human induced pluripotent stem cells. J Cell Biochem. 2020; 121(5-6): 3185-3196.
30. Stani C, Vaccari L, Mitri E, Birarda G. FTIR investigation of the secondary structure of type I collagen: New insight into the amide III band. Spectrochim Acta A Mol Biomol Spectrosc. 2020; 229: 118006.
31. Koons GL, Diba M, Mikos AG. Materials design for bone-tissue engineering. Nat Rev Mater. 2020; 5(8): 584-603.
32. Salerno A, Netti PA. Review on bioinspired design of ECM-mimicking scaffolds by computer-aided assembly of cell-free and cell laden micro-modules. J Funct Biomater. 2023; 14(2): 101.
33. Capuana E, Lopresti F, Ceraulo M, La Carrubba V. Poly-l-Lactic Acid (PLLA)-based biomaterials for regenerative medicine: a review on processing and applications. Polymers (Basel). 2022; 14(6): 1153.
34. Liao S, Tamura K, Zhu Y, Wang W, Uo M, Akasaka T, et al. Human neutrophils reaction to the biodegraded nano-hydroxyapatite/collagen and nano-hydroxyapatite/collagen/poly(L-lactic acid) composites. J Biomed Mater Res A. 2006; 76(4): 820-825.
35. Dong C, Lv Y. Application of collagen scaffold in tissue engineering: recent advances and new perspectives. Polymers (Basel). 2016; 8(2): 42.
36. Ielo I, Calabrese G, De Luca G, Conoci S. Recent advances in hydroxyapatite-based biocomposites for bone tissue regeneration in orthopedics. Int J Mol Sci. 2022; 23(17): 9721.
37. Zhu Y, Goh C, Shrestha A. Biomaterial properties modulating bone regeneration. Macromol Biosci. 2021; 21(4): e2000365.
38. Ali Akbari Ghavimi S, Allen BN, Stromsdorfer JL, Kramer JS, Li X, Ulery BD. Calcium and phosphate ions as simple signaling molecules with versatile osteoinductivity. Biomed Mater. 2018; 13(5): 055005.
39. Yanagida H, Okada M, Masuda M, Narama I, Nakano S, Kitao S, et al. Preparation and in vitro/in vivo evaluations of dimpled poly(L-lactic acid) fibers mixed/coated with hydroxyapatite nanocrystals. J Artif Organs. 2011; 14(4): 331-341.
40. Yanagida H, Okada M, Masuda M, Ueki M, Narama I, Kitao S, et al. Cell adhesion and tissue response to hydroxyapatite nanocrystal-coated poly(L-lactic acid) fabric. J Biosci Bioeng. 2009; 108(3): 235-243.